Metabolomics analysis of antiquitin deficiency in cultured human cells and plasma: Relevance to pyridoxine-dependent epilepsy

Crowther, Lisa M ; Poms, Martin ; Zandl-Lang, Martina ; Abela, Lucia ; Hartmann, Hans ; Seiler, Michelle ; Mathis, Déborah ; Plecko, Barbara

DOI: https://doi.org/10.1002/jimd.12569

Received: 2 April 2021 | Revised: 9 October 2022 | Accepted: 10 October 2022

DOI: 10.1002/jimd.12569

ORIGINAL ARTICLE

JIMD SSIEM WILEY

Metabolomics analysis of antiquitin deficiency in cultured human cells and plasma: Relevance to pyridoxine-dependent epilepsy

Lisa M. Crowther[1,2,3] | **Martin Poms**[1,2,3,4] | **Martina Zandl-Lang**[5] | **Lucia Abela**[1,6] | **Hans Hartmann**[7] | **Michelle Seiler**[8] | **Déborah Mathis**[4,9] | **Barbara Plecko**[1,2,3,5]

[1]Division of Child Neurology, University Children's Hospital Zurich, Zurich, Switzerland

[2]CRC Clinical Research Center, University Children's Hospital Zurich, Zurich, Switzerland

[3]Radiz—Rare Disease Intiative Zurich, Clinical Research Priority Program for Rare Diseases, University of Zurich, Zurich, Switzerland

[4]Department of Clinical Chemistry and Biochemistry, University Children's Hospital Zurich, Zurich, Switzerland

[5]Department of Pediatrics and Adolescent Medicine, Division of General Pediatrics, Medical University of Graz, Graz, Austria

[6]Molecular Neurosciences, Developmental Neuroscience, UCL Institute of Child Health, London, UK

[7]Department of Pediatric Kidney, Liver and Metabolic Diseases, Hannover Medical School, Hannover, Germany

[8]Pediatric Emergency Department, University Children's Hospital Zurich, Zurich, Switzerland

[9]University Institute of Clinical Chemistry, Inselspital, Bern University Hospital, University of Bern, Bern, Switzerland

Correspondence
Barbara Plecko, Department of Pediatrics and Adolescent Medicine, Division of General Pediatrics, University Childrens' Hospital Graz, Medical University of Graz, Auenbruggerplatz 34/2, 8036, Graz, Austria.
Email: barbara.plecko@medunigraz.at; deborah.mathis@insel.ch

Funding information
Hartmann Müller-Stiftung für Medizinische Forschung, Grant/Award Number: 1802; Schweizerischer Nationalfonds zur Förderung der

Abstract

Deficiency of antiquitin (α-aminoadipic semialdehyde dehydrogenase), an enzyme involved in lysine degradation and encoded by *ALDH7A1*, is the major cause of vitamin B_6-dependent epilepsy (PDE-ALDH7A1). Despite seizure control with high dose pyridoxine (PN), developmental delay still occurs in approximately 70% of patients. We aimed to investigate metabolic perturbations due to possible previously unidentified roles of antiquitin, which may contribute to developmental delay, as well as metabolic effects of high dose pyridoxine supplementation reflecting the high doses used for seizure control in patients with PDE-ALDH7A1. Untargeted metabolomics by high resolution mass spectrometry (HRMS) was used to analyze plasma of patients with PDE-ALDH7A1 and

Abbreviations: AAA, α-aminoadipic acid; AADAT/KAT2, kynurenine/alpha-aminoadipate aminotransferase; AASA, α-aminoadipic semialdehyde; AASS, α-aminoadipic semialdehyde synthase; ATQ, antiquitin; CRYM/KR, μ-crystallin/ketimine reductase; gDNA, genomic DNA; IS, internal standard; LC–MS/MS, liquid chromatography–tandem mass spectrometry; LRD, lysine-restricted diet; MPE, molar percent enrichment; n.d., not detectable; n.s., not significant; NPC, neural progenitor cells; P5CR, pyrroline-5-carboxylate reductase; P6C, Δ^1-piperideine-6-carboxylate; PA, pipecolic acid; PIPOX, pipecolic acid oxidase; PLP, pyridoxal 5′-phosphate; PN, pyridoxine; sgRNA, single guide RNA; UHPLC-HRMS, ultrahigh performance liquid chromatography-high resolution mass spectrometry.

Lisa M. Crowther and Martin Poms contributed equally to this work.

Déborah Mathis and Barbara Plecko share the last authorship.

Wissenschaftlichen Forschung, Grant/Award Number: 320030_163302

Communicating Editor: Ron A Wevers

two independently generated lines of cultured ReNcell CX human neuronal progenitor cells (NPCs) with CRISPR/Cas mediated antiquitin deficiency. Accumulation of lysine pathway metabolites in antiquitin-deficient NPCs and western-blot analysis confirmed knockdown of *ALDH7A1*. Metabolomics analysis of antiquitin-deficient NPCs in conditions of lysine restriction and PN supplementation identified changes in metabolites related to the transmethylation and transsulfuration pathways and osmolytes, indicating a possible unrecognized role of antiquitin outside the lysine degradation pathway. Analysis of plasma samples of PN treated patients with PDE-ALDH7A1 and antiquitin-deficient NPCs cultured in conditions comparable to the patient plasma samples demonstrated perturbation of metabolites of the gamma-glutamyl cycle, suggesting potential oxidative stress-related effects in PN-treated patients with PDE-ALDH7A1. We postulate that a model of human NPCs with CRISPR/Cas mediated antiquitin deficiency is well suited to characterize previously unreported roles of antiquitin, relevant to this most prevalent form of pyridoxine-dependent epilepsy.

KEYWORDS

antiquitin deficiency, lysine catabolism, metabolomics, NPCs, PDE-ALDH7A1, pyridoxine

1 | INTRODUCTION

Antiquitin (α-aminoadipic semialdehyde dehydrogenase), encoded by *ALDH7A1*, is an enzyme in the lysine degradation pathway that converts α-aminoadipic semialdehyde (AASA) to α-aminoadipic acid (AAA) (Figure 1). Antiquitin deficiency leads to accumulation of AASA and its cyclic form Δ^1-piperideine-6-carboxylate (P6C), that likely inactivates pyridoxal 5′-phosphate (PLP) and leads to an imbalance of cerebral neurotransmitter- and amino acid metabolism, and pyridoxine (PN)-dependent epilepsy (PDE-ALDH7A1).[1]

70% of patients with PDE-ALDH7A1 suffer from developmental delay,[1–3] which may result from accumulation of the neurotoxic compound AASA/P6C, however a wide range of developmental outcome has been seen for the same mutations under Western diets.[1,4,5] Add-on treatment, including lysine-restricted diet (LRD), and/or arginine supplementation, have been shown to decrease AASA/P6C but so far only short term data on improved developmental outcome have been reported.[6–9]

Recently antiquitin deficiency was studied in *Aldh7a1* knockout zebrafish[10,11] as well as *Aldh7a1* knockout mice[12] by targeted metabolite analysis. Zebrafish models have the disadvantage that whole larvae do not allow tissue specific analysis, which is necessary to study lysine metabolism. The mouse model bears species-specific differences of the lysine degradation pathway,[13–18] best illustrated by elevated AAA in *Aldh7a1* knockout mice[12] which is not found in human with PDE-ALDH7A1. It is therefore clear that examining the effects of antiquitin deficiency in human cell types of neural origin is of utmost importance.

We hypothesized that antiquitin deficiency may lead to previously unidentified perturbations in metabolic pathways outside of the lysine degradation pathway, and unrelated to vitamin B_6 availability. This could be due to promiscuity of antiquitin function, or to secondary inhibition of other enzymes by toxic compounds such as AASA/P6C. Any such effects of antiquitin deficiency would have great impact on understanding the pathophysiology and on novel treatment options.

For a comprehensive and untargeted analysis of global metabolic effects of antiquitin deficiency, we used an ultrahigh performance liquid chromatography-high resolution mass spectrometry (UHPLC-HRMS) based metabolomics platform. We generated a human cell culture model by CRISPR/Cas genome editing in an immortalized human neural progenitor cell line (ReNcell CX neural progenitor cells, NPCs) derived from the cortical region of human fetal brain. We cultured the cells in different conditions and compared as follows:

1. Antiquitin-deficient NPCs and control NPCs were cultured in *high lysine media*, to confirm expected effects of antiquitin deficiency in the lysine degradation pathway.
2. Antiquitin-deficient NPCs and control NPCs were cultured in *lysine-free media supplemented with PN* to

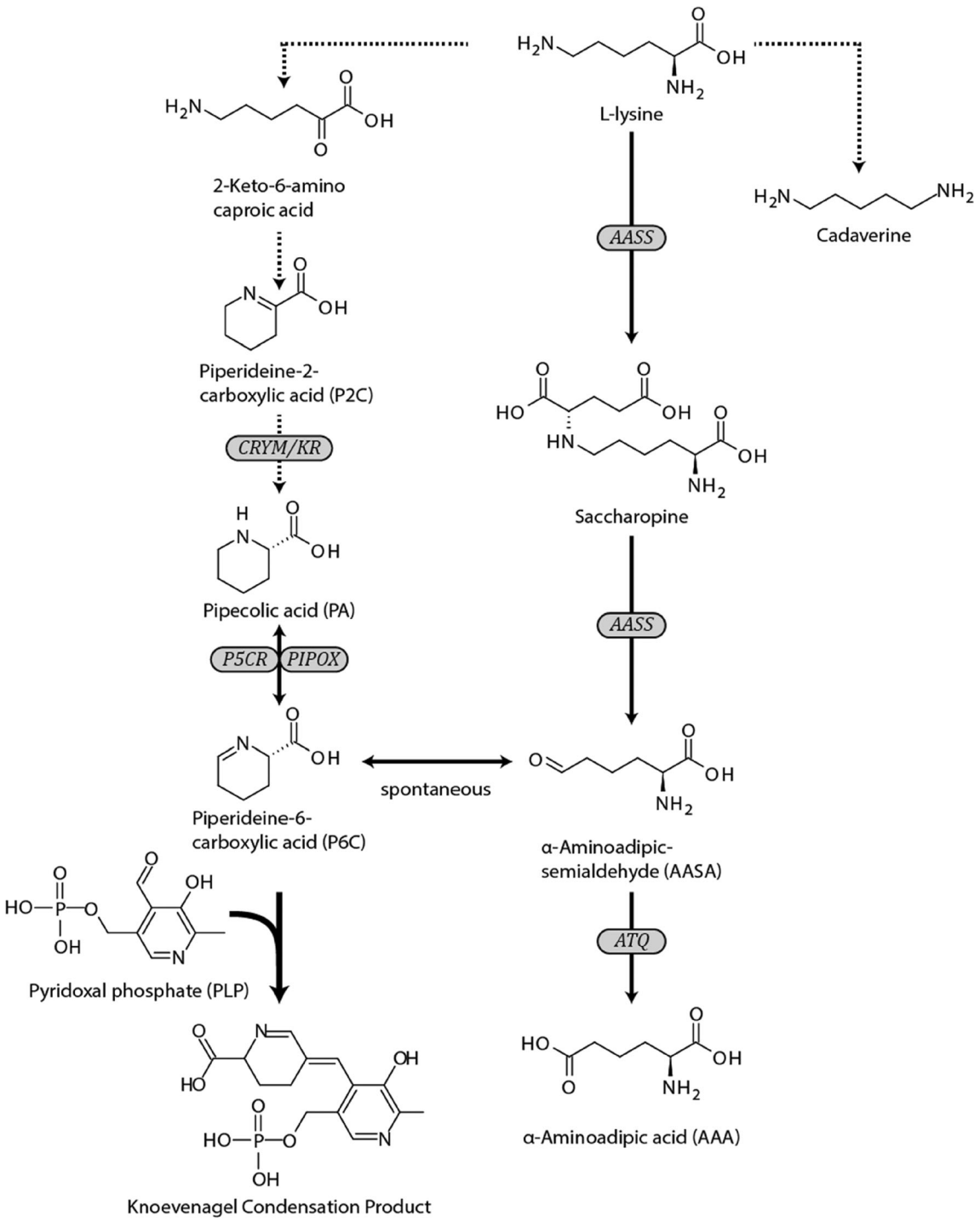

FIGURE 1 Overview of lysine degradation pathway. Dashed lines indicate proposed reactions for which no enzymes have yet been identified in human. The proposed structure of the Knoevenagel condensation product has only been shown in vitro. AASS α-aminoadipic semialdehyde synthase; ATQ antiquitin (α-aminoadipic semialdehyde dehydrogenase); CRYM/KR, μ-crystallin/ketimine reductase; PIPOX pipecolic acid oxidase; P5CR pyrroline-5-carboxylase reductase

eliminate accumulation of lysine pathway metabolites and vitamin B_6 deficiency, and to identify changes distinct from the previously identified role of antiquitin in the lysine degradation pathway.

3. Antiquitin-deficient NPCs were cultured in *high PN media or with normal cell culture concentrations of PN*. This intra-cell type comparison was performed to identify effects of PN supplementation in antiquitin deficiency.
4. Finally, we also compared plasma of patients with PDE-ALDH7A1 with controls and investigated whether similar patterns were obtained from comparison of antiquitin-deficient cells with controls in treatment-mimicking conditions.

2 | METHODS

2.1 | Generation, isolation, and characterization of antiquitin^{null} NPCs

ReNcell CX human neuronal progenitor cells (NPCs) were transfected with Cas9 protein and guide RNA (LabOmics, Belgium) targeting *ALDH7A1*, using the Neon nucleofector (Life Technologies) according to the manufacturer's protocol. Guide RNA was designed to target exon 2 of *ALDH7A1* (designated gRNA ex2), with the sequence 5′ CTCGTTGTTAGCAGGGCAATAGG 3′ or exon 14 with the sequence 5′ AAAAGTCTCTGTGTGTG-CAATGG 3′ (designated gRNA ex14).

Successful gene disruption was confirmed by sequencing genomic DNA (gDNA) extracted from the colonies of NPCs obtained from single cell clonal expansion. The likeliest off-target sites were determined using the CCTOP online tool for identification of potential off target effects[19] and gDNA from each knockout and control NPC colony selected for experiments was sequenced to confirm absence of off-target effects. Antiquitin protein expression of each colony was analyzed by western blot analysis. All details are given in the Supplementary Information.

2.2 | Cell culture

ReNcell CX human neural progenitor cells (Millipore, Billerica, MA) (NPCs) were cultured according to the manufacturers' directions. Cells were seeded on laminin-coated glass coverslips (20 μg/ml) at a density of 5000 cells per cm^2 in Rencell media, or for lysine restriction experiments in custom lysine-free DMEM-F12 (3:1) supplemented with B27 (2%), 2 μg/mL Heparin, FGF (20 ng/ml), and EGF (20 ng/ml). For experiments analyzing effects of high levels of lysine, media was supplemented to final lysine concentration 1.18 mg/mL (10 times the usual concentration in 3,1 DMEM-F12 media). For experiments analyzing effects of high PN, PN was supplemented to 18 mg/mL PN (9 times the usual cell culture media concentration).

Cells were harvested for metabolomics analysis with modifications of published protocols.[20] In brief, coverslips were removed from cell culture wells using forceps, and washed briefly in 37°C ddH_20, then placed in ice cold 50% MeOH in a 6-well-plate kept on ice. Cells were scraped into the 50% MeOH and transferred to 1.5 ml tubes and stored at −20°C until further processing. Samples were then sonicated for 15 seconds (Bandelin Sonorex) and centrifuged for 15 min, 4°C at 14500 rpm following DNA quantification by Hoechst assay.

2.3 | Hoechst assay

To account for differences in efficiency of cell transfer during harvesting, we used fluorescence-based DNA quantification to estimate the number of cells in the harvested extracts, as previously described.[21] In brief, 5 μl of each sample or standard was incubated with 20 μg/ml Hoechst dye in PBS (80 μl per well) for 30 min, after what fluorescence was measured (360/460 nm). A standard curve of fluorescence versus cell number was generated using standards containing known cell numbers of the same cell type prepared in 50% MeOH following trypsinisation, cell counting, and sonication. For the metabolomics samples, cells per ml were estimated by comparison to the standard curve, and exact volumes for each sample were calculated to ensure the same amount of cell lysate material in each analysis. Cell extracts were then prepared as described below (Section 2.5).

2.4 | Patient sample preparation

Blood from patients with PDE-ALDH7A1 ($n = 13$) and age-matched controls (non-PDE-ALDH7A1, on regular diet) was taken in lithium-heparin tubes, centrifuged, the plasma separated and frozen immediately and stored at −80°C. Shipping was carried out on dry ice where applicable. For MS analysis, 100 μl of sample were deproteinated by adding 400 μl of ice-cold methanol, vortexed, and centrifuged for 10 min at 14 500 rpm. The supernatant was evaporated and stored at −80°C until analysis.

2.5 | Quantification of lysine degradation metabolites

Quantitative analysis of the lysine degradation intermediates PA and AASA/P6C in cell extracts was performed using a liquid chromatography–tandem mass spectrometry system (LC–MS/MS, Thermo UHPLC Ultimate 3000 XRS coupled to an AB SCIEX 5500 TripleQuad) as previously described.[22]

2.6 | Metabolomics

Dried samples were dissolved in 50% MeOH, including 0.1 mM uracil-5-d_1 as an internal standard (IS), which was used as qualitative control to detect potential inconsistencies or outliers with regard to chromatography, injection, and ionization. Chromatographic separation was achieved using a 2.1 × 100 mm Kinetex HILIC column (Phenomenex, Torrance, CA). Elution was achieved

by running a stepwise gradient from 100% buffer B (acetonitrile/water 95:5, 0.1% formic acid, 5 mM ammonium formate) to 100% buffer A (acetonitrile/water 50:50, 0.1% formic acid, 5 mM ammonium formate), 0%–50% A over 12 min, 50%–100% A over 3 min with a total runtime of 20 min. Flow rate was kept constant at 0.4 ml/min with a column temperature of 30°C.

Mass spectra were acquired using a heated electrospray ionization (HESI) source of a Q-Exactive high resolution, accurate mass spectrometer (Thermo Scientific, Waltham, MS). Mass spectra were recorded in positive ion mode with the MS detector in full-scan mode (Full-MS) in the scan-range 67–1000 *m/z* with data-dependent (dd-MS2) acquisition of fragment ions from the top-5 most abundant ions per scan. Initially, all experiments were also run in negative mode. However, those analyses only yielded very limited total (<2000) and limited significant features (<10) compared to positive mode and were not pursued further.

Samples were measured as technical triplicates and outliers were detected and removed if the variation in the IS signal was too large (80%–120% recovery of the IS) or if they could clearly be classified as outliers in the multivariate analysis. No quality control was used between batches as only samples from the same experiment were compared.

2.7 | Analysis and statistics

Raw data was assembled using Xcalibur (4.1, Thermo) and converted to .mzXML format using the MSconvert.exe program.[23] Data preprocessing, including total ion current normalization, baseline correction, and peak alignment as well as peak picking was achieved utilizing the XCMS package[24] in R[25] (x64, v3.3.1).

To identify significantly altered metabolites, the UHPLC-HRMS runs for each condition were compared using multivariate and univariate analysis. Multivariate analyses were carried out in R using the muma software package.[26] After noise filtering, data imputation, total ion current normalization and Pareto scaling, significantly altered features were analyzed. The features (*m/z* values with a specific retention time) that exhibited the largest changes were mined utilizing a pathway- and network-based approach using the mummichog algorithm[27] and confirmed by comparison to an internal database or retention time analysis and fragment pattern matching against the Metlin,[28] HMDB[29] and mzCloud databases. Fold changes were calculated as the ratio of mean peak areas between two groups in a given experiment. *p*-Values were calculated by independent two-tailed *t*-tests on the area under the curve.

3 | RESULTS

3.1 | Generation and characterization of antiquitin-deficient neural progenitor cell model

CRISPR/Cas mediated mutations were generated by transfection of NPCs with Cas9 protein, and single-guide RNA (sgRNA) targeting exon 2 or exon 14 of the *Aldh7a1* gene. Sanger sequencing of gDNA from each single-cell colony confirmed gene disruption (Figure S1). Sequencing of the highest scoring potential exonic off-target sites, as determined by the CCTop online prediction tool,[19] demonstrated no mutations in any of the isolated colonies. These included CD27, UNK, RP11, and TRIM44 (Figure S4).

Western blot analysis confirmed the loss of antiquitin expression in two colonies expanded from CRISPR gRNA exon 2-transfected NPCs (ex2 (1) and ex2 (3)) and decreased antiquitin expression in the third colony (ex2 (2)). Loss of antiquitin expression was also observed in two colonies expanded from CRISPR gRNA exon 14 (ex14 (1) and ex14 (2)) (Figure 2).

We excluded the colonies obtained from transfection with sgRNA targeting exon 14 due to unexpected sequence alterations over a larger region in these cells, detected by Sanger sequencing.

Indels in the *Aldh7a1* gene of Ex2 (1) and Ex2 (3) clones were further analyzed using the CRISP-ID tool which deconvolutes Sanger sequencing data to be read as subsequences corresponding to indels within individual alleles.[30] CRISP-ID analysis demonstrated that colonies ex2 (1) and ex2 (3) had biallelic indels (Figure S2). We confirmed that

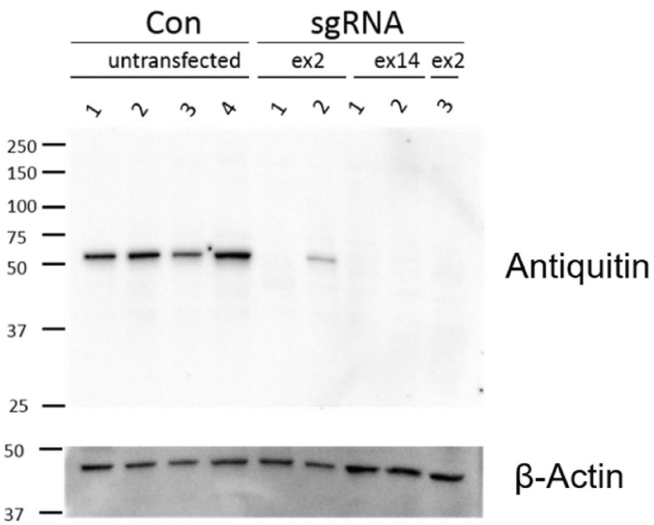

FIGURE 2 Western blot analysis showing antiquitin and β-Actin expression in control (untransfected) and CRISPR/Cas transfected colonies of neuronal progenitor cells (NPCs) following single cell expansion

the differentiation status of the antiquitin knockout NPCs was unchanged from control untransfected colonies by western blot of Nestin, GFAP, and Tuj1 (Figure S3).

The two colonies with biallelic indels in exon 2 and loss of antiquitin protein expression (ex2 (1) and ex2 (3) hereafter referred to as ATQ-1 and ATQ-3) were selected for further analysis.

3.2 | Quantitative analysis of PA and AASA/P6C in antiquitin-deficient NPC colonies: Confirmation of lysine degradation metabolite changes

Control and antiquitin-deficient NPCs were harvested after incubation in media containing high levels of lysine. Quantitative analysis showed accumulation of PA and AASA/P6C in the antiquitin-deficient NPC colonies but not in control cells (Figure S5). Therefore, CRISPR/Cas9 mediated antiquitin deficiency led to expected downstream changes in the lysine degradation pathway.

Quantitative analysis of PA and AASA/P6C was also performed on antiquitin-deficient and control cells cultured in lysine-free media. In these conditions, accumulation of lysine metabolites AASA/P6C and PA was not observed (Figure S5). This validates the use of such conditions to study changes outside the lysine degradation pathway in antiquitin-deficient NPCs.

3.3 | Metabolic profiles of antiquitin deficiency using untargeted metabolomics

An untargeted metabolomics approach was used to identify differences in the metabolome by pairwise comparison as reported below.

It has to be noted that this approach yields only semi-quantitative results, potentially leading to considerable differences in reported fold changes between experiments. Especially the utilization of Pareto scaling, which was employed in order to emphasize small and medium fold changes, leads to a greater decrease of large fold changes resulting in wider variations between experiments. Significant *p*-value thresholds were therefore calculated individually for each experiment using Bonferroni correction. Depending on the number of total observed features, corrected *p*-value thresholds were calculated to be between $p = 0.00005$ and $p = 0.00001$. In the tables the highest *p*-value for significantly altered experiments are given. Identifiable metabolites that did not pass the corrected *p*-value threshold, but showed a trend (with a *p*-value between 0.05 and the corrected *p*-value cut-off), are also mentioned in the comment column of the tables in order to not miss the detection of potentially important metabolomic changes.

Typically, about 30–100 significantly altered features were detected per comparison out of 1200 and 1900 total features. However, only a fraction of observed features could be uniquely identified, and these features were subsequently tracked in all other comparisons. Tables shown include all identified metabolites for the various comparisons that show significant differences in the majority of experiments (each comparison was repeated in independent experiments between three to six times).

3.3.1 | Metabolomic profiles of antiquitin-deficient NPCs and controls cultured in high lysine media—confirmation of detection of lysine degradation pathway perturbations

As expected, untargeted metabolomics identified decreased AAA and increased pipecolic acid in antiquitin-deficient cells compared to controls in conditions of high lysine. Furthermore, we detected decreased hypotaurine and betaine, and increased choline in antiquitin-deficient NPCs compared to controls in these conditions (Table 1A). Interestingly, intra-cell type comparison revealed an increase in cadaverine in high lysine conditions compared to cells cultured without lysine (Figure S6). The fold change was higher in controls than in antiquitin-deficient NPCs.

3.3.2 | Metabolomic profiles of antiquitin-deficient NPCs compared to controls cultured with lysine restriction and PN supplementation—Study of the effects of antiquitin deficiency outside the lysine degradation pathway

Antiquitin-deficient NPCs were compared to controls in conditions of lysine-free media supplemented with PN. In those conditions, with undetectable AASA/P6C and PA accumulation but high PN concentration, we detected increased taurine, hypotaurine and choline by untargeted metabolomics analysis of antiquitin-deficient NPCs compared to controls (Table 1B).

3.3.3 | Metabolomic profiles of antiquitin-deficient NPCs cultured with high PN compared to normal PN—Study of the effects of PN supplementation in antiquitin-deficient NPCs

As expected, untargeted metabolomics identified PN and pyridoxal as highly increased in PN supplemented

TABLE 1 Significantly altered metabolites in antiquitin-deficient neuronal progenitor cells (NPCs) compared to control NPCs (A) cultured in high-lysine containing media; (B) cultured in lysine-free and high pyridoxine (PN) media

(A) High lysine					
Compound	***m/z***	**Ion**	**Fold change**	***p*-Value**	**Comments**
α-Aminoadipate	162.077	M + H	0.02–0.1	<1.00 E−005	5/6 significant, 1 trending (p 0.0002, 0.001)
Betaine	118.086	M + H	0.4–0.6	<1.00 E−005	2/6 significant, 4 n.d.
Choline	104.107	M+	1.4–2.3	<1.00 E−005	3/6 significant, 1 trending (0.00003), 2 n.s.
Hypotaurine	110.027	M + H	0.6	<1.00 E−008	2/6 significant, 2 trending (p 0.000058, 0.01), 2 n.s.
Pipecolic acid	130.086	M + H	6	<1.00 E−06	2/6 significant, 4 n.d.
(B) Lysine-free, high PN					
Compound	***m/z***	**Ion**	**Fold change**	***p*-Value**	**Comments**
Choline	104.107	M+	1.3	1.00 E−005	2/5 significant, 2 trending (p 0.0006, 0.01), 1 n.s.
Hypotaurine	110.027	M + H	1.6–4.2	1.00 E−006	3/5 significant, 1 trending (p 0.006), 1 n.s.
Taurine	126.022	M + H	2.4–2.6	1.00 E−005	2/5 significant, 2 trending (p 0.0004, 0.0004), 1 n.s.

Note: Values given in the *p*-value column correspond to the highest *p*-value (independent two-tailed *t*-tests) of significantly altered experiments. Comments include the number of significantly altered experiments as well as trending *p*-values. Not significant and not detectable metabolites are represented as n.s. and n.d., respectively.

antiquitin-deficient NPCs compared to non-supplemented cells (Table 2). Furthermore, we identified decreased betaine, choline, creatine, glutamate, glutamine, glycine, hypotaurine, leucine, lysine, oxo-proline, putrescine, serine, and taurine with PN supplementation, with the *p*-value reaching the Bonferroni corrected significance threshold in at least one experiment, and the same change trending in other experiments (*p*-values 0.05 or below). Several of these are metabolites of the gamma-glutamyl cycle, including glutamate, glycine, and oxo-proline.

3.3.4 | Metabolomic profiles of patient plasma with PDE-ALDH7A1 versus control plasma, and antiquitin-deficient NPCs versus control NPCs in "treatment-mimicking conditions"

Untargeted metabolomics was performed using plasma of patients with PDE-ALDH7A1 treated with PN, with or without LRD, and compared to control plasma samples of age matched individuals without PN supplementation on a regular diet (Table 3). Patients with PDE-ALDH7A1 ($n = 13$, age range 7 months to 11 years) were split into four groups depending on age and diet (<4 years/LRD [$n = 4$]; <4 years/no LRD [$n = 3$]; >4 years/LRD [$n = 3$]; >4 years/no LRD [$n = 3$]).

In all four groups of patients with PDE-ALDH7A1, pyridoxal and PA were increased as expected, and creatine, cysteine, glutamine, guanidinoacetate, hypotaurine, taurine, leucine, and oxo-proline were decreased. *Lysine* was higher in patients <4 years of age without LRD compared to controls, while patients <4 years of age on LRD had lysine concentrations comparable to age matched controls. In patients >4 years of age lysine was decreased compared to age matched controls regardless of LRD. *Glutamate* was increased in patients with PDE-ALDH7A1 compared to controls in the younger patient group only, regardless of LRD. *Choline* was found to be decreased in patients on LRD compared to controls in both age groups (Table 3).

For comparison of the patient plasma analysis to the antiquitin-deficient NPC culture model, we also performed untargeted metabolomics analysis of antiquitin-deficient NPCs compared to control NPCs, using culture conditions mimicking the treatment conditions of the PDE-ALDH7A1 and control cohorts. Antiquitin-deficient cells were thus cultured with or without lysine with PN supplementation and were compared to control cells cultured with normal conditions for lysine and PN ("untreated conditions"). This comparison confirmed metabolite changes that were also present in patient plasma under similar treatment conditions such as decreased taurine, hypotaurine and glutamine (with and without lysine), decreased serine (without lysine) and decreased guanidinoacetate (with lysine) (Tables 3, ST1 and ST2).

4 | DISCUSSION

Antiquitin deficiency is the most common type of vitamin B_6-dependent epilepsy. It is not well understood why

TABLE 2 Significantly altered features in antiquitin-deficient neuronal progenitor cells (NPCs) incubated in pyridoxine (PN)-supplemented media, compared to cells cultured in media without supplementation

Compound	*m/z*	Ion	Fold change	*p*-Value	Comments
Betaine	118.086	M + H	0.6–0.7	1.00 E−005	2/5 significant, 1 n.s., 2 n.d.
Choline	104.107	M+	0.7	1.00 E−007	1/5 significant, 2 trending (0.004, 0.001), 2 n.s.
Creatine	132.077	M + H	0.4–0.5	1.00 E−004	2/5 significant, 2 trending (p 0.02, 0.00003), 1 n.s.
Glutamate	102.050	M-H_2O-CO + H	0.4–0.5	1.00 E−004	2/5 significant, 2 trending (p 0.04, 0.0001), 1 n.s.
Glutamine	130.050	M-NH_3 + H	0.5–0.7	1.00 E−004	2/5 significant, 1 trending (0.04), 1 n.s., 1 n.d.
	147.077	M + H	0.7	1.00 E−006	1/5 significant, 3 trending (0.002, 0.0001, 0.00003), 1 n.s.
Glycine	76.039	M + H	0.4	1.00 E−006	1/5 significant, 4 trending (0.01, 0.002, 0.004, 0.0004)
Hypotaurine	110.027	M + H	0.4–0.5	1.00 E−006	3/5 significant, 1 trending (p 0.02), 1 n.s.
Leucine	86.096	M-H_2O-CO + H	0.6	1.00 E−006	1/5 significant, 2 trending (0.0002, 0.0003), 2 n.s.
	132.101	M + H	0.65	1.00 E−011	1/5 significant, 2 trending (0.01, 0.0002), 2 n.s.
Lysine	130.086	M-NH_3 + H	0.6	1.00 E−006	1/5 significant, 2 trending (0.04, 0.02), 2 n.s.
	147.112	M + H	0.6	1.00 E−006	1/5 significant, 1 trending (0.03), 3 n.s.
Oxo-proline	130.049	M + H	0.6	1.00 E−007	1/5 significant, 2 trending (p 0.004, 0.03), 2 n.s.
Putrescine	72.081	M-NH_3 + H	0.4–0.5	1.00 E−006	2/5 significant, 2 trending (p 0.004, 0.002), 1 n.s.
	89.107	M + H	0.5	1.00 E−009	1/5 significant, 2 trending (p 0.008, 0.0001), 2 n.s.
Pyridoxal	168.065	M + H	4–7	1.00 E−004	5/5 significant
Pyridoxine	134.060	M-H_4O_2 + H	19–73	1.00 E−006	5/5 significant
	152.070	M-H_2O + H	19–113	1.00 E−006	5/5 significant
	170.081	M + H	15–120	1.00 E−006	5/5 significant
	171.084	M + ^{13}C + H	10–25	1.00 E−006	5/5 significant
	192.062	M + Na	13–55	1.00 E−006	4/5 significant, 1 n.d.
	208.036	M + K	10–69	1.00 E−005	5/5 significant
Serine	88.039	M-H_2O + H	0.6	1.00 E−004	1/5 significant, 2 trending (0.003, 0.006), 2 n.s.
	106.050	M + H	0.5–0.55	1.00 E−004	2/5 significant, 3 trending (p 0.01, 0.004, 0.0005)
Taurine	126.022	M + H	0.4–05	1.00 E−004	3/5 significant, 2 trending (p 0.02, 0.005)

Note: Values given in the *p*-value column correspond to the highest *p*-value (independent two-tailed *t*-tests) of significantly altered experiments. Comments include the number of significantly altered experiments as well as trending *p*-values. Not significant and not detectable metabolites are represented as n.s. and n.d., respectively.

70% of patients have developmental delay which does not correlate with time of diagnosis and treatment, or genotype.[1–3] We therefore examined whether antiquitin may be involved in other metabolic pathways aside from its already well-established role in lysine degradation. This could be by promiscuity of the enzymatic activity of antiquitin or by secondary inhibition due to accumulating toxic metabolites, such as AASA/P6C. Previously unreported perturbation in those pathways may contribute to developmental delay seen in patients with PDE-ALDH7A1 on vitamin B_6 therapy despite early and successful seizure control. Furthermore, identification of remote metabolic effects may open additional treatment options.

Untargeted metabolomics has the potential to unravel unexpected changes and to detect secondary effects of antiquitin deficiency outside of the lysine degradation pathway. However, it has to be noted that this approach is very sensitive and changes can vary appreciably between experiments. The influence of diet, age, gender, environment, medication, and genetic background impedes standardized conditions when analyzing the metabolomics profile in plasma samples of patients, which leads to a large number of metabolic variations that are not disease specific. Also, sufficient numbers of patient samples are difficult to obtain due to the low prevalence of rare disorders. To circumvent these difficulties and gain insight into antiquitin deficiency in various conditions mimicking treatment conditions, we used untargeted metabolomics analysis in CRISPR/Cas mediated *ALDH7A1* knockout NPCs. Use of clones derived from single cells following CRISPR/Cas knockout of

TABLE 3 Significantly altered (bold) and trending (*italic*) features in plasma of patients with PDE-ALDH7A1, separated into four groups (<4 years and >4 years, as well as add-on lysine-restricted diet [LRD] or regular diet) in comparison to age-matched controls

			Fold change			
			<4 years		>4 years	
Compound	***m/z***	**Ion**	**LRD**	**No LRD**	**LRD**	**No LRD**
Alanine	90.055	M + H				*1.31*
Arginine	217.153	M + ACN + H		*0.38*	**0.21**	**0.17**
	197.100	M + Na			*0.84*	*0.77*
	175.118	M + H	*2.57*			*0.51*
Choline	104.107	M + H	*0.68*		**0.82**	
Creatine	133.069	M + ^{13}C + H	**0.09**	*0.15*	*0.12*	*0.16*
	170.031	M + K			**0.70**	
Cysteine	144.013	M + Na	*0.15*	*0.16*	**0.42**	**0.35**
Glutamate	170.061	M + Na	**2.52**	*2.68*		
Glutamine	147.076	M + H	*0.51*	*0.69*		
	185.032	M + K	**0.23**	**0.22**	**0.46**	**0.35**
Glycine	76.039	M + H		*0.61*		*1.67*
Guanidinoacetate	140.042	M + Na			**0.46**	*0.74*
	156.016	M + K			**0.21**	*0.45*
	160.096	M + ACN + H	*0.15*	**0.15**		
	118.061	M + H	*0.49*	*0.66*	*0.68*	
Hypotaurine	110.027	M + H	**0.27**	*0.27*	*0.62*	*0.44*
Leucine	132.101	M + H	*0.55*		*0.79*	*0.77*
	86.096	M-H_2O-CO + H	*0.55*		*0.74*	**0.72**
Lysine	130.086	M-NH_3 + H		**1.46**	**0.42**	**0.55**
	147.112	M + H		*1.60*	**0.40**	**0.54**
	185.067	M + K		*1.62*	**0.26**	**0.28**
	84.081	M-NH_3-H2O-CO + H		*1.50*		**0.51**
Oxo-proline	130.050	M + H	**0.02**	**0.07**	*0.61*	
Phenylalanine	166.085	M + H	*0.45*	*0.63*	*0.76*	
Pipecolic acid	130.086	M + H	**2.56**	*4.87*	*1.55*	
Pyridoxal	168.065	M + H	*40.41*	**36.35**	*27.39*	*6.42*
Serine	106.050	M + H	**0.45**	*0.66*		
Taurine	126.022	M + H	**0.23**	*0.38*	*0.75*	
	148.004	M + Na	**0.12**	*0.23*	*0.72*	

Note: Changes that are also significant in antiquitin-deficient versus control NPCs in "treatment mimicking conditions" (Tables ST1 and ST2) are indicated by gray backgrounds. Blank fields indicate that the metabolite was not significantly altered in those conditions.

ALDH7A1 (and comparison to corresponding single cell clonal controls) minimizes non-disease specific metabolic variations and allows investigations using standardized conditions. We used NPCs derived from human fetal brain, as species differences and cell-type differences have been shown in enzyme activities of the lysine degradation pathway and antiquitin deficiency.[13–18,22]

4.1 | Metabolomic changes in the lysine degradation pathway in antiquitin deficiency

The use of cell culture models allowed us to study the metabolome of antiquitin-deficient cells compared to control cells under standardized conditions, such as

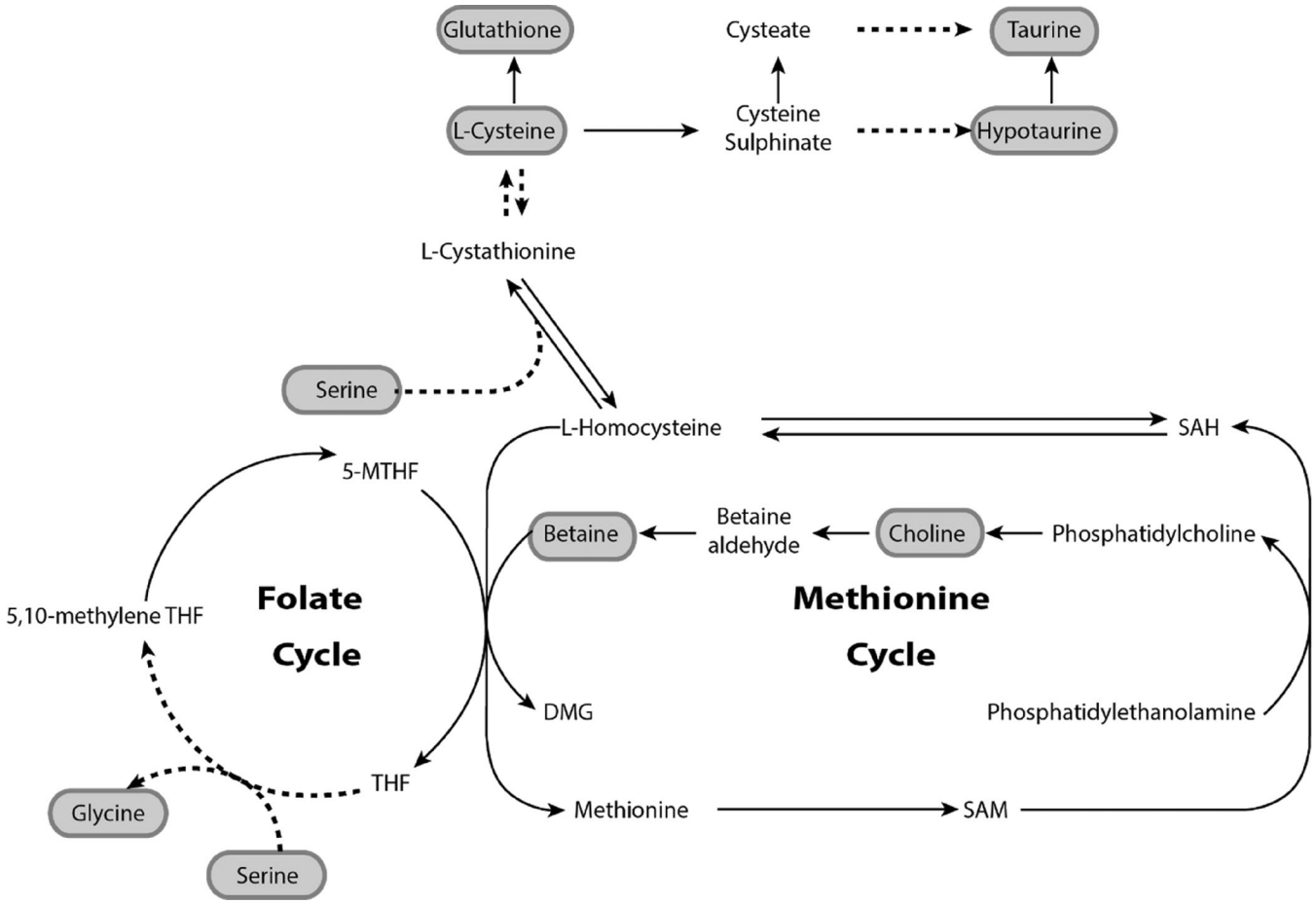

FIGURE 3 Overview of the folate cycle and methionine cycle. Metabolites that are significantly changed in any of the cell culture experiments are indicated by gray boxes. Pathways that require vitamin B_6 as a cofactor[36] are indicated by dashed lines. 5-methyltetrahydrofolate (5-MTHF); 5,10-methylene tetrahydrofolate (5,10 methylene THF); S-adenosyl methionine (SAM); S-adenosyl homocysteine (SAH)

pretreatment state (high lysine without PN supplementation) and treatment state (lysine-free with PN supplementation). We confirmed functional deficiency in the two CRISPR/Cas edited antiquitin-deficient NPC lines first by quantitative analysis of AASA/P6C and PA demonstrating accumulation of these lysine degradation metabolites, and secondly by untargeted metabolomics analysis which showed decreased levels of AAA after the enzymatic block. Other disease specific biomarkers such as AASA/P6C as well as the newly reported 2 S,6 S-/2 S,6R-oxopopylpiperidine-2-carboxylic acid and 6-oxopiperidine-2-carboxylic acid[31,32] could not be detected with this experimental approach, most likely due to different chromatography (HILIC vs. reverse-phase) or due to the fact that only the positive ionization mode was utilized. In accordance with expected effects of antiquitin deficiency related to the lysine degradation pathway, we observed lysine-dependent effects on cadaverine in NPCs, and age-dependent changes in lysine in patient plasma.

Cadaverine: Interestingly, untargeted metabolomics analysis in antiquitin-deficient and control NPCs showed an increase of cadaverine with high lysine, suggesting the decarboxylation of lysine as a potential third lysine degradation pathway (Figure 1). Mammalian cells have previously been shown to metabolize lysine to cadaverine by decarboxylation[33] and the degradation of lysine to cadaverine has been observed in mouse brain.[34] Bacterial lysine decarboxylase has been shown to be PLP dependent,[35] although the corresponding enzyme in humans has not yet been identified. This suggests that decarboxylation may represent a possible alternative pathway of lysine degradation in mammalian cells and would be an interesting topic of further studies. Furthermore, the fold change in cadaverine was higher in controls cells than in antiquitin-deficient NPCs, possibly due to enhanced activity of AASS in case of antiquitin deficiency (see above).

Age-dependent changes in lysine: Metabolomic analysis of patient plasma with PDE-ALDH7A1 compared to

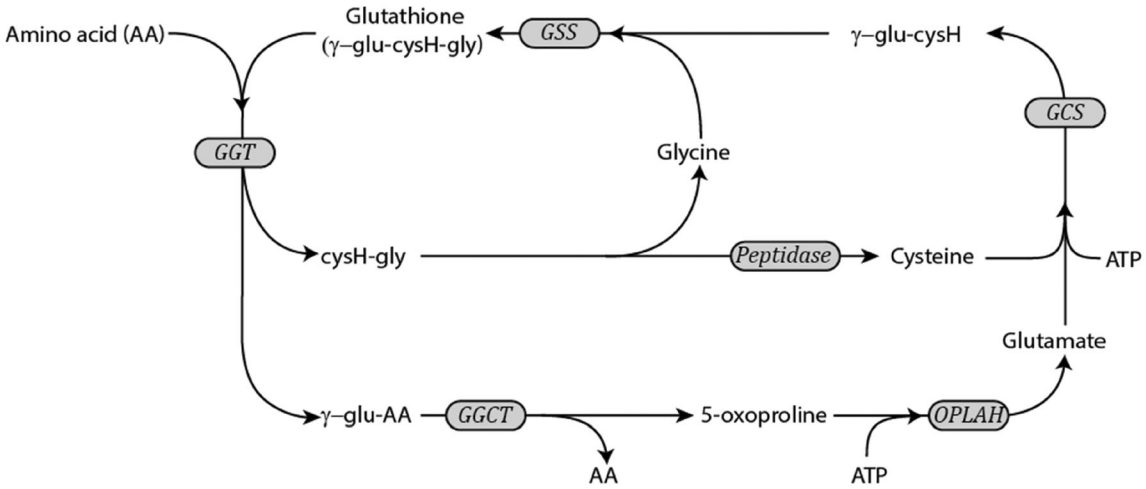

FIGURE 4 The gamma-glutamyl cycle, adapted from Larsson A. (1990) Disorders of the Gamma Glutamyl Cycle. In: Fernandes J., Saudubray JM., Tada K. (eds) Inborn Metabolic Diseases. Springer, Berlin, Heidelberg.[37] Glutathione synthetase (GSS), gamma-glutamyl transferase (GGT), gamma-glutamylcyclotransferase (GGCT), 5-oxoprolinase (OPLAH), glutamate cystein lygase (GCS)

controls demonstrated age-dependent changes in lysine. In patients with PDE-ALDH7A1 on a regular diet, lysine was slightly higher in patients <4 years of age compared to age matched controls, and this effect was normalized in patients on LRD. Interestingly, in the older age group, lysine was lower in patients with PDE-ALDH7A1 compared to age matched controls, in both treatment groups (LRD and regular diet). This decrease in lysine could be due to enhanced activity of AASS in case of antiquitin deficiency, as shown in fibroblasts by previous isotopic tracing studies of our group,[22] which is also supported by the recent finding of low lysine and high saccharopine levels in brain of antiquitin-deficient mice.[12] Further studies are needed to examine this effect in patients with antiquitin deficiency and to show if potential effects on AASS activity are age-dependent, species-specific and/or cell-type dependent.

4.2 | Secondary metabolomic changes: folate and methionine cycle

When considering the metabolic differences detected in antiquitin-deficient cells compared to control cells in the various conditions examined in this study, many of the identified altered metabolites such as betaine, choline, taurine, and hypotaurine are connected via the folate cycle and methionine cycle as shown in Figure 3. Vitamin B_6 is required as a cofactor for many of these reactions (represented with dashed lines), indicating the importance of controlling vitamin B_6 availability when analyzing the effects of antiquitin deficiency.

Reduction of *betaine* in antiquitin-deficient NPCs compared to controls was only detected in conditions of high lysine and no longer in lysine-free conditions. Furthermore, reduced betaine and choline was observed in high PN-treated antiquitin-deficient NPCs compared to normal PN. This may suggest secondary effects of accumulating lysine and PN metabolites on betaine metabolism. Antiquitin has previously been shown to metabolize betaine aldehyde to betaine in vitro, although the role of antiquitin in this pathway has not been studied extensively.

The effect of antiquitin deficiency on *hypotaurine* and taurine we observed in human NPCs was also dependent on lysine availability. Hypotaurine was decreased in antiquitin-deficient cells compared to controls in conditions of high lysine but increased in lysine-free conditions, as did taurine. This may indicate a promiscuous role of antiquitin in taurine/hypotaurine metabolism. In zebrafish with CRISPR/Cas mediated antiquitin deficiency, decreased taurine levels were identified in extracts from deep-frozen larvae (11 dpf),[10] however no details on the lysine supply at the time of sampling was provided.

4.3 | Secondary metabolomic changes: Osmolytes

Many osmolytes were altered in antiquitin-deficient cells and patient plasma compared to controls, including betaine, choline, taurine, hypotaurine, creatine, glutamate, glutamine, serine, and glycine. Although the role of osmolytes in the brain is not well elucidated, it is becoming an increasingly recognized field of interest. In plants, antiquitin has been proposed to have an osmoregulatory role although to our knowledge, this role has so far not been demonstrated in animals.

Glycine and serine were recently reported to be decreased in vitamin B_6-deficient Neuro-2a cells and glycine was decreased in brain tissue of antiquitin-deficient mice.[12] However, effects of vitamin B_6-deficiency on glycine and serine appear to be species specific, as in human conditions of vitamin B_6-deficiency, glycine and serine are increased or unchanged. Glycine and serine were increased in plasma of vitamin B_6-deficient human patients, as was glycine in CSF of non-supplemented PNPO-deficient patients, and in vitamin B_6-deprived HepG2 cells. This is most likely due to vitamin B_6-dependent reactions in the glycine cleavage system. We detected decreased glycine and serine in PN-supplemented patients with PDE-ALDH7A1 and NPCs when compared to non-PN supplemented NPC controls.

4.4 | Metabolomic changes due to PN treatment: cells and patient plasma

The active form of vitamin B_6 is a cofactor for many enzymatic reactions but the metabolic effects of high-dose PN treatment have not yet been studied extensively. We detected decreased levels of glutamine, glycine, hypotaurine, serine, and taurine in antiquitin-deficient-NPCs cultured in high PN compared to normal PN. These metabolites were also decreased in plasma of PN-treated patient with PDE-ALDH7A1 compared to non-PN supplemented age-matched individuals, and in antiquitin-deficient NPCs compared to non-PN supplemented control NPCs (mimicking patient plasma conditions).

Interestingly, many of the PN-dependent changes that we observed in our cell model included metabolites of the *gamma-glutamyl cycle* (Figure 4). Decreased oxo-proline, glutamate, and glycine was detected in antiquitin-deficient NPCs cultured in PN versus controls. Similarly, in plasma of PN-treated patients with PDE-ALDH7A1 we identified lowered cysteine, glycine, and oxo-proline compared to controls. Effects of vitamin B_6 deficiency and PN supplementation on glutathione and oxidative stress have been examined previously. However, similar studies examining the effect of long-term supplementation with therapeutic doses of PN (15–30 mg/kg/day in neonates, up to 200–300 mg/day in infants and toddlers, and 500 mg/day in adults) have not been reported. Perturbation of glutathione-system-associated metabolites in PN-treated NPCs and patients might indicate oxidative stress-related effects in PN treated antiquitin deficiency. In addition, the antiquitin protein itself has been postulated as a protective agent against toxic aldehydes and the recently characterized *ALDH7A1* knockout mouse model demonstrated accumulation of methionine sulfoxide in brain of knockout and heterozygous mice, indicating increased ROS content.[12]

5 | CONCLUSION

In summary, we established a CRISPR/Cas9 mediated antiquitin-deficient human NPC model, and were able to investigate conditions of PN and lysine supplementation mimicking patient treatment conditions. In addition to the previously characterized changes in the lysine degradation pathway, we observed changes in intermediates of the folate and methionine cycles and in osmolytes, indicating a possible unrecognized role of antiquitin outside the lysine degradation pathway. Furthermore, analysis of plasma samples of PN treated patients with PDE-ALDH7A1 and antiquitin-deficient NPCs cultured in comparable conditions, demonstrated perturbation of metabolites of the gamma-glutamyl cycle, which suggest potential oxidative stress-related effects in PN-treated patients with PDE-ALDH7A1. The main goal of an untargeted metabolomics study is to cover a large portion of the metabolome, which requires a certain preselection in possibly observable metabolites with the limitation to observe changes in only relatively abundant metabolites. As a next step, the findings of this study should be confirmed by quantitative targeted LC–MS analysis on selected metabolites. Further investigations into the effects of long term, high dose PN on oxidative stress pathways may be important to choose the most beneficial doses for seizure reduction as well as oxidative stress control, to ensure optimal outcomes for patients with PDE-ALDH7A1.

AUTHOR CONTRIBUTIONS

Lisa M. Crowther: Drafted the study design, conducted all cell culture and molecular biology experiments, interpreted the data and results and drafted the manuscript. **Martin Poms**: Measured, analyzed and interpreted metabolomics data and drafted the manuscript. **Martina Zandl-Lang**: Assisted in data interpretation and critically reviewed the manuscript. **Lucia Abela**: Gave input into drafting and critically reviewed the manuscript. **Hans Hartmann**: Contributed plasma samples of patients with PDE-ALDH7A1 including details on their current treatment and critically reviewed the manuscript. **Michelle Seiler**: Collected control plasma samples for metabolome analysis and critically reviewed the manuscript. **Déborah Mathis**: Performed the quantitative analyses, interpreted the data and drafted the manuscript. **Barbara Plecko**: Gave substantial input to the study design, data interpretation and to the manuscript.

FUNDING INFORMATION

This project has been funded by the Swiss National Fund (SNF), grant number 320030_163302 and by the Hartmann-Müller Stiftung grant 1802.

CONFLICT OF INTEREST

Lisa M. Crowther, Martin Poms, Martina Zandl-Lang, Lucia Abela, Hans Hartmann, Michelle Seiler, Déborah Mathis, and Barbara Plecko declare that they have no conflict of interest.

DATA AVAILABILITY STATEMENT

The data that support the findings of this study are available from the corresponding author upon reasonable request.

ETHICS STATEMENT

All procedures followed were in accordance with the ethical standards of the responsible committee on human experimentation (institutional and national) and with the Helsinki Declaration of 1975, as revised in 2000.

INFORMED CONSENT

Informed consent was obtained from all patients for being included in the study.

ORCID

Martin Poms https://orcid.org/0000-0002-4426-314X
Déborah Mathis https://orcid.org/0000-0002-2326-7782
Barbara Plecko https://orcid.org/0000-0002-3203-1325

REFERENCES

1. Mills PB, Footitt EJ, Mills KA, et al. Genotypic and phenotypic spectrum of pyridoxine-dependent epilepsy (ALDH7A1 deficiency). *Brain*. 2010;133:2148-2159.
2. Basura GJ, Hagland SP, Wiltse AM, Gospe SM Jr. Clinical features and the management of pyridoxine-dependent and pyridoxine-responsive seizures: review of 63 North American cases submitted to a patient registry. *Eur J Pediatr*. 2009;168:697-704.
3. Bok LA, Halbertsma FJ, Houterman S, et al. Long-term outcome in pyridoxine-dependent epilepsy. *Dev Med Child Neurol*. 2012;54:849-854.
4. Coulter-Mackie MB, Tiebout S, van Karnebeek C, Stockler S. Overexpression of recombinant human antiquitin in *E. coli*: partial enzyme activity in selected ALDH7A1 missense mutations associated with pyridoxine-dependent epilepsy. *Mol Genet Metab*. 2014;111:462-466.
5. Tlili A, Hamida Hentati N, Chaabane R, Gargouri A, Fakhfakh F. Pyridoxine-dependent epilepsy in Tunisia is caused by a founder missense mutation of the ALDH7A1 gene. *Gene*. 2013;518:242-245.
6. Mercimek-Mahmutoglu S, Cordeiro D, Cruz V, et al. Novel therapy for pyridoxine dependent epilepsy due to ALDH7A1 genetic defect: L-arginine supplementation alternative to lysine-restricted diet. *Eur J Paediatr Neurol*. 2014;18:741-746.
7. Mercimek-Mahmutoglu S, Corderio D, Nagy L, et al. Lysine-restricted diet and mild cerebral serotonin deficiency in a patient with pyridoxine-dependent epilepsy caused by ALDH7A1 genetic defect. *Mol Genet Metab Rep*. 2014;1:124-128.
8. van Karnebeek CDM, Stockler-Ipsiroglu S, Jaggumantri S, et al. Lysine restricted diet for pyridoxine-dependent epilepsy: first evidence and future trials. *Mol Genet Metab*. 2012;107:335-344.
9. Coughlin CR, van Karnebeek CDM, Al-Herttani W, et al. Triple therapy with pyridoxine, arginine supplementation and dietary lysine restriction in pyridoxine-dependent epilepsy: neurodevelopmental outcome. *Mol Genet Metab*. 2015;116:35-43.
10. Pena IA, Roussel Y, Daniel K, et al. Pyridoxine-dependent epilepsy in zebrafish caused by Aldh7a1 deficiency. *Genetics*. 2017;207:1501-1518.
11. Zabinyakov N, Bullivant G, Cao F, et al. Characterization of the first knock-out aldh7a1 zebrafish model for pyridoxine-dependent epilepsy using CRISPR-Cas9 technology. *PLoS One*. 2017;12:e0186645.
12. Al-Shekaili HH, Petkau TL, Pena I, et al. A novel mouse model for pyridoxine-dependent epilepsy due to antiquitin deficiency. *Hum Mol Genet*. 2020;29:3266-3284.
13. Grove J, Henderson LM. The metabolism of D- and L-lysine in the intact rat, perfused liver and liver mitochondria. *Biochim Biophys Acta*. 1968;165:113-120.
14. Posset R, Opp S, Struys EA, et al. Understanding cerebral L-lysine metabolism: the role of L-pipecolate metabolism in Gcdh-deficient mice as a model for glutaric aciduria type I. *J Inherit Metab Dis*. 2015;38:265-272.
15. Zaar K, Angermuller S, Volkl A, Fahimi HD. Pipecolic acid is oxidized by renal and hepatic peroxisomes. Implications for Zellweger's cerebro-hepato-renal syndrome (CHRS). *Exp Cell Res*. 1986;164:267-271.
16. Mihalik SJ, Rhead WJ. L-pipecolic acid oxidation in the rabbit and cynomolgus monkey. Evidence for differing organellar locations and cofactor requirements in each species. *J Biol Chem*. 1989;264:2509-2517.
17. Ghadimi H, Chou WS, Kesner L. Biosynthesis of saccharopine and pipecolic acid from L- and DL-14 C-lysine by human and dog liver in vitro. *Biochem Med*. 1971;5:56-66.
18. Rao VV, Pan X, Chang YF. Developmental changes of L-lysine-ketoglutarate reductase in rat brain and liver. *Comp Biochem Physiol B*. 1992;103:221-224.
19. Stemmer M, Thumberger T, Del Sol Keyer M, Wittbrodt J, Mateo JL. CCTop: an intuitive, flexible and reliable CRISPR/Cas9 target prediction tool. *PLoS One*. 2015;10:e0124633.
20. Martano G, Delmotte N, Kiefer P, et al. Fast sampling method for mammalian cell metabolic analyses using liquid chromatography-mass spectrometry. *Nat Protoc*. 2015;10:1-11.
21. Muschet C, Möller G, Prehn C, de Angelis MH, Adamski J, Tokarz J. Removing the bottlenecks of cell culture metabolomics: fast normalization procedure, correlation of metabolites to cell number, and impact of the cell harvesting method. *Metabolomics*. 2016;12:151.
22. Crowther LM, Mathis D, Poms M, Plecko B. New insights into human lysine degradation pathways with relevance to pyridoxine-dependent epilepsy due to antiquitin deficiency. *J Inherit Metab Dis*. 2019;42:620-628.
23. Kessner D, Chambers M, Burke R, Agus D, Mallick P. ProteoWizard: open source software for rapid proteomics tools development. *Bioinformatics*. 2008;24:2534-2536.

24. Tautenhahn R, Bottcher C, Neumann S. Highly sensitive feature detection for high resolution LC/MS. *BMC Bioinform*. 2008;9:504-520.
25. R Core Team. *R: A Language and Environment for Statistical Computing*. R Foundation for Statistical Computing; 2016.
26. Gaude, E.C F, Spiliotopoulos D, Spitaleri A, et al. muma, an R package for metabolomics univariate and multivariate statistical analysis. *Curr Metab*. 2013;1:180-189.
27. Li S, Park Y, Duraisingham S, et al. Predicting network activity from high throughput metabolomics. *PLoS Comput Biol*. 2013; 9:e1003123.
28. Guijas C, Montenegro-Burke JR, Domingo-Almenara X, et al. METLIN: a technology platform for identifying knowns and unknowns. *Anal Chem*. 2018;90:3156-3164.
29. Wishart DS, Jewison T, Guo AC, et al. HMDB 3.0—the human metabolome database in 2013. *Nucleic Acids Res*. 2013;41:D801-D807.
30. Dehairs J, Talebi A, Cherifi Y, Swinnen JV. CRISP-ID: decoding CRISPR mediated indels by Sanger sequencing. *Sci Rep*. 2016;6:28973.
31. Wempe MF, Kumar A, Kumar V, et al. Identification of a novel biomarker for pyridoxine-dependent epilepsy: implications for newborn screening. *J Inherit Metab Dis*. 2019;42:565-574.
32. Engelke UF, van Outersterp RE, Merx J et al. Untargeted metabolomics and infrared ion spectroscopy identify biomarkers for pyridoxine-dependent epilepsy. *J Clin Invest*. 2021;131:e148272.
33. Hawel L 3rd, Tjandrawinata RR, Fukumoto GH, Byus CV. Biosynthesis and selective export of 1,5-diaminopentane (cadaverine) in mycoplasma-free cultured mammalian cells. *J Biol Chem*. 1994;269:7412-7418.
34. Schmidt-Glenewinkel T, Nomura Y, Giacobini E. The conversion of lysine into piperidine, cadaverine, and pipecolic acid in the brain and other organs of the mouse. *Neurochem Res*. 1977; 2:619-637.
35. Gale EF, Epps HM. Studies on bacterial amino-acid decarboxylases: 1. l(+)-lysine decarboxylase. *Biochem J*. 1944; 38:232-242.
36. Percudani R, Peracchi A. The B6 database: a tool for the description and classification of vitamin B6-dependent enzymatic activities and of the corresponding protein families. *BMC Bioinform*. 2009;10:273.
37. Fernandes J, Saudubray J-M, Van den Berghe G, Tada K, Buist NRM. *Inborn Metabolic Diseases*. Springer; 1995.

SUPPORTING INFORMATION

Additional supporting information can be found online in the Supporting Information section at the end of this article.

How to cite this article: Crowther LM, Poms M, Zandl-Lang M, et al. Metabolomics analysis of antiquitin deficiency in cultured human cells and plasma: Relevance to pyridoxine-dependent epilepsy. *J Inherit Metab Dis*. 2022;1-14. doi:10.1002/jimd.12569